3D-QSAR and Docking Studies of Selective GSK-3β Inhibitors. Comparison with a Thieno[2,3-*b*]pyrrolizinone Derivative, a New Potential Lead for GSK-3β Ligands

Elodie Lescot, Ronan Bureau,* Jana Sopkova-de Oliveira Santos, Christophe Rochais, Vincent Lisowski, Jean-Charles Lancelot, and Sylvain Rault

Centre d'Etudes et de Recherche sur le Médicament de Normandie, Université de Basse-Normandie, 5, rue Vaubénard, 14032 Caen, France

Received January 7, 2005

The three-dimensional structures of 3-anilino-4-arylmaleimides, selective GSK-3β inhibitors, were correlated to their biological affinities by 3D-QSAR studies (CoMFA method). The cocrystallographic data of GSK-3β vs 3-anilino-4-arylmaleimide allowed us to compare 3D-QSAR results to experimental intermolecular interactions. The results of the CoMFA analysis did not really correspond to the interactions recorded in the active site, but they characterized fundamental features (areas of the active site) of the interactions ligand−receptor. These studies were the starting point to analyze a new GSK-3β ligand, a thieno[2,3-*b*]pyrrolizinone derivative. This comparison based on docking and simulation approaches allowed us to confirm one preferential orientation of this ligand inside the active site, explaining the relationship with the reference 3-anilino-4-arylmaleimide derivatives and its biological affinity.

INTRODUCTION

The serine threonine kinase glycogen synthase kinase-3 (GSK-3) is ubiquitously expressed in mammalian tissues and interferes with numerous signaling processes. Two isoforms of GSK-3 exist (α, β) and are high homologous in their catalytic domain (97% homology) but mainly diverge at the N terminus. Both GSK-3α and GSK-3β contain a conserved N-terminal serine residue (S21 for GSK-3α and S9 for GSK-3β) whose phosphorylation is important for the regulation of the enzymatic activity.[1,2] The phosphorylation of proteins by GSK-3β is an important link in signaling pathways that regulate cell differentiation, cellular growth and proliferation, metabolic processes, apoptosis control, inflammation, and mechanisms involved in neuronal function.[3,4] GSK-3β is also known to phosphorylate the microtubules associated with the protein tau in mammalian cells.[5] Hyperphosphorylation of protein tau is an early event in neurodegenerative conditions such as Alzheimer's disease. Therefore, small molecule inhibitors of GSK-3β may have a therapeutic potential in numerous human diseases.

Several classes of ATP-competitive GSK-3β inhibitors have been described recently, such as maleimides derivatives,[6−9] indirubins,[10] paullone,[11,12] staurosporine,[13] aloisines,[14] and the marine sponge hymenialdisine.[15] X-ray structures of GSK-3β have also been described[16−18] in the last years, and recently cocrystallographic data of GSK-3β with selective and nonselective ATP mimetic inhibitors have been published.[19]

Currently, within the research program on GSK-3β developed the past few years in our laboratory, preliminary tests showed that the compound **1**, a thieno[2,3-*b*]pyrrolizinone (Figure 1), appeared to have an interesting affinity[20] ($IC_{50} = 1.6\ \mu M$). This compound was recently described as an antitubulin agent.[21]

* Corresponding author phone: (33)2-31-43-69-73; fax: (33)2-31-93-11-88; e-mail: bureau@pharmacie.unicaen.fr.

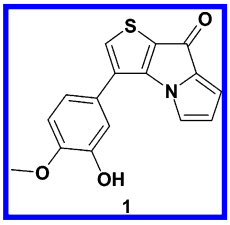

Figure 1. Structure of the thieno[2,3-*b*]pyrrolizinone derivative.

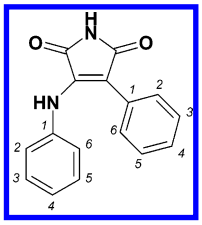

Figure 2. Structure of 3-anilino-4-arylmaleimide derivatives.

To understand its biological affinity, the first 3D-QSAR study on previous published selective GSK-3β inhibitors was carried out. We chose the maleimides derivatives,[6] selective inhibitors against GSK-3β (Figure 2), with an affinity of ca. 20 nM for the best one. We then compared 3D-QSAR results with cocrystallographic data GSK-3β/3-anilino-4-arylmaleimide in order to understand and complete the available structural information. Finally, these structural information were linked to the position of compound **1** into the active site obtained by docking.

METHODS AND MATERIALS

Data Set. The compounds published by Smith et al. in 2001[6] were used as training set for CoMFA calculation. Among the compounds in this publication, 74 were considered for the 3D-QSAR analysis (Table 1). The GSK-3β IC_{50} converted to pIC_{50} (-log IC_{50}) were used as dependent variables in the CoMFA calculations. These biological data cover two logarithmic units (5.64 to 7.70).

10.1021/ci050008y CCC: $30.25
Published on Web 03/25/2005

Table 1. Structures and Experimental and Predicted pIC_{50} Values for Training Set

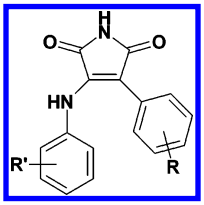

	R	R′	pIC_{50}	cross-validation			R	R′	pIC_{50}	cross-validation	
				calcd	residuals					calcd	residuals
2	H	H	6.28	6.24	0.04	34	3-nitro	3-chloro-4-hydroxy	7.23	7.14	0.09
3	4-chloro	H	6.29	6.22	0.07	35	2-chloro	3-chloro-4-hydroxy	6.82	6.81	0.01
4	2-chloro	H	6.67	6.43	0.24	36	2-methoxy	3-chloro-4-hydroxy	6.86	6.93	−0.07
5	2-methoxy	H	6.67	6.65	0.02	37	4-chloro	3-chloro-4-hydroxy	6.76	6.72	0.04
6	3-nitro	H	6.85	6.83	0.02	38	2-chloro	3,5-dichloro-4-hydroxy	7.09	7.15	−0.06
7	4-methoxy	H	6.41	6.34	0.07	39	2-methoxy	3,5-dichloro-4-hydroxy	7.09	7.31	−0.22
8	2-nitro	3-chloro	6.98	6.95	0.03	40	2-nitro	3,5-dichloro-4-hydroxy	7.28	7.49	−0.21
9	3-nitro	3-chloro	7.15	6.99	0.16	41	3-chloro	3,5-dichloro-4-hydroxy	7.24	7.07	0.17
10	4-chloro	3-chloro	6.35	6.43	−0.08	42	3-nitro	3,5-dichloro-4-hydroxy	7.70	7.5	0.2
11	H	3-chloro	6.52	6.57	−0.05	43	4-chloro	3,5-dichloro-4-hydroxy	7.04	6.95	0.09
12	2-chloro	3-chloro	6.71	6.68	0.03	44	4-methoxy	3,5-dichloro-4-hydroxy	7.08	6.97	0.11
13	2-methoxy	3-choro	6.94	6.96	−0.02	45	4-nitro	3,5-dichloro-4-hydroxy	7.15	7.11	0.04
14	3-methoxy	3-chloro	6.59	6.58	0.01	46	H	3,5-dichloro-4-hydroxy	6.83	6.97	−0.14
15	4-methoxy	3-chloro	6.81	6.56	0.25	47	3-methoxy	3,5-dichloro-4-hydroxy	6.85	6.91	−0.06
16	H	3-hydroxy	6.15	6.28	−0.13	48	2-chloro	4-chloro-3-carboxy	7.13	7.1	0.03
17	3-chloro	3-hydroxy	5.83	6.37	−0.54	49	2-nitro	4-chloro-3-carboxy	7.55	7.5	0.05
18	3-methoxy	3-hydroxy	6.33	6.35	−0.02	50	3-chloro	4-chloro-3-carboxy	7.12	7.08	0.04
19	4-chloro	3-hydroxy	6.39	6.28	0.11	51	3-methoxy	4-chloro-3-carboxy	7.07	7.1	−0.03
20	4-methoxy	3-hydroxy	6.32	6.35	−0.03	52	3-nitro	4-chloro-3-carboxy	7.59	7.49	0.1
21	2-chloro	3-hydroxy	6.43	6.41	0.02	53	4-chloro	4-chloro-3-carboxy	6.96	6.98	−0.02
22	2-methoxy	3-hydroxy	6.59	6.71	−0.12	54	H	4-chloro-3-carboxy	6.84	6.96	−0.12
23	2-nitro	3-hydroxy	6.60	6.78	−0.18	55	H	4-Sme	6.39	6.4	−0.01
24	3-nitro	3-hydroxy	6.63	6.79	−0.16	56	2-methoxy	4-Sme	6.96	6.82	0.14
25	3-nitro	3-carboxy	7.10	7.19	−0.09	57	3-chloro	4-Sme	6.27	6.53	−0.26
26	H	3-carboxy	6.54	6.59	−0.05	58	4-chloro	4-Sme	6.28	6.45	−0.17
27	2-chloro	3-carboxy	6.87	6.85	0.02	59	2-chloro	4-Sme	6.79	6.61	0.18
28	3-chloro	3-carboxy	6.87	6.77	0.1	60	3-methoxy	4-Sme	6.69	6.54	0.15
29	3-methoxy	3-carboxy	6.71	6.77	−0.06	61	3-nitro	4-Sme	6.82	6.96	−0.14
30	4-chloro	3-carboxy	6.73	6.7	0.03	62	4-methoxy	4-Sme	6.61	6.47	0.14
31	4-methoxy	3-carboxy	6.67	6.76	−0.09	63	4-nitro	4-Sme	6.41	6.5	−0.09
32	2-nitro	3-chloro-4-hydroxy	6.98	7.13	−0.15	64	3-nitro	4-hydroxy	6.91	6.85	0.06
33	3-chloro	3-chloro-4-hydroxy	7.03	6.7	0.33	65	4-chloro	4-hydroxy	6.50	6.38	0.12

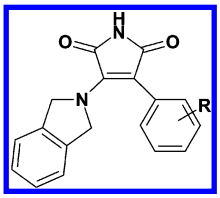

	R	pIC_{50}	cross-validation			R	pIC_{50}	cross-validation	
			calcd	residuals				calcd	residuals
66	2-chloro	6.47	6.38	0.09	70	3-nitro	6.79	6.77	0.02
67	2-methoxy	6.73	6.59	0.14	71	4-chloro	5.85	6.19	−0.34
68	2-nitro	6.88	6.72	0.16	72	4-methoxy	6.16	6.24	−0.08
69	3-chloro	6.34	6.3	0.04					

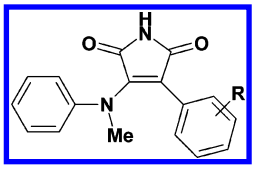

	R	pIC_{50}	cross-validation			R	pIC_{50}	cross-validation	
			calcd	residuals				calcd	residuals
73	H	5.58	5.48	0.1	75	4-chloro	5.54	5.47	0.07
74	3-NO_2	5.85	5.96	−0.11					

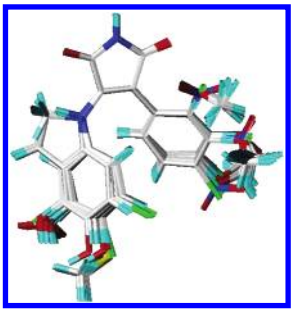

Figure 3. Superimposition of 3-anilino-4-arylmaleimide derivatives.

Molecular Modeling. The three-dimensional structures of all compounds in the training set were obtained using the SYBYL program package.[22] Partial atomic charges were calculated by the Gasteiger−Huckel method, and energy minimizations were performed using the Tripos force field[23] with a distance dependent dielectric and the Powell conjugate gradient algorithm (convergence criterion of 0.05 kcal/mol).

Alignment Definition. The conformation of **50** cocrystallized with GSK-3β was the basic structure for this alignment (PDB ID: 1Q4L[19]). Each molecule was initially aligned on the maleimide group, and then the dihedral angles were fixed by considering values of the reference compound. Finally, all substituents were oriented in the same way (Figure 3) within the substitution series.

CoMFA Analysis. 3D cubic lattice box with a grid spacing of 2 Å and 1 Å were created around the aligned molecules. Steric and electrostatic CoMFA fields were calculated using Csp^3 probe atom (charge +1). The default cutoff (30 kcal/mol) was applied to both fields by considering the "smooth" method. To determine the optimal number of component, samples Partial Least Square (PLS) algorithm was used.[24] The optimum number of components (ONC) was used for deriving the subsequent PLS[25] models (first minimum in the standard error). Cross-validation was performed using the "leave-one-out" method with a column filtering of 2.0 kcal/mol. Finally, nonvalidated models were produced, and conventional correlation coefficient r^2 and standard error s were computed.

Alternatives to calculate the CoMFA fields (standard method) were also considered. The "box" option was used, which consists of replacing the probe atom by eight probe atoms (making the corners of a cube) centered on the coordinates of the original one. The interactions between each probe atom and the target molecule are calculated, and the average value was assigned to the original probe coordinates. For the cutoff, another method called "abrupt" was also tested instead of the "smooth" approach.[22] We have also investigated[26] the dependence between the resulting q^2 values and the orientation of rigidly aligned molecules (CoMFA fields: standard method). The variation of the q^2 values are represented in Figure 4.

X-ray Data. Atomic coordinates for the GSK-3β complexes with 3-anilino-4-arylmaleimide and indirubin-3′-monoxime inhibitors, used for our modeling study, have been deposited in the Protein Data Bank[19] with resolutions of 2.77 Å and 2.1 Å (PDB ID: 1Q4L and 1Q41, respectively).

Docking Studies. The original ligand as well as the water molecules were removed from the coordinates set. The Gold program[27] was employed to generate an ensemble of docked

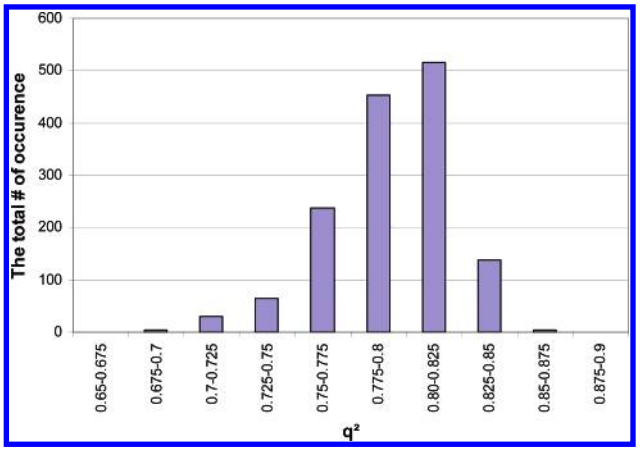

Figure 4. The q^2 values (Csp^3 as probe atom) observed for different orientations of the 74 compounds. The molecular aggregate was systematically rotated by 30° at a time around x, y, and z axes.

conformations. The genetic operators were 100 for the population size, 1.1 for the selection, 5 for the number of subpopulations, 100 000 for the maximum number of genetic applications, and 2 for the size of the niche used to increase population diversity. The weights were chosen so that crossover mutations were applied with equal probability (95/95 for the values), and migration was applied 5% of the time.

Energy Minimization of the Complex in Solution. Energy minimizations after docking were performed with the CHARMM software[28] (Chemistry and HARvard Molecular Mechanics) using the parameter[29] set 22. The complex model was placed in a 500 ps preequilibrated water box (type TIP3P[30]). All water molecules closer than 2.8 Å from protein were discarded. To derive parameters for the compound **1**, ab initio quantum-chemical calculations were performed on the isolated molecule using the program Jaguar[31] (RHF/6-31G**) and MOPAC (AM1). The atomic partial charges were derived using Mulliken population analysis. The molecular mechanics force field determined for the compound **1** was used to minimize the molecular geometry. A 0.25 Å RMSD for **1** after minimization compared to the X-ray structure[21] was obtained. The van der Waals interactions were truncated using a switching function between 11 Å and 14 Å, and the electrostatic interactions were smoothly brought to zero at 14 Å using a shifting function. The two complex models were minimized to an RMS energy gradient lower than 10^{-3} kcal/(mol·Å).

RESULTS AND DISCUSSION

CoMFA Results. Four different methods were carried out for the calculation of the steric and electrostatic fields ("abrupt" or "smooth" toward "none" or "box") with two grid spacing. The statistical results from cross-validation studies (q^2 values) are summarized in Table 2. Steric fields are highly correlated with the biological data whichever approach is taken. Inclusion of electrostatic fields led to a slight improvement of the statistics. Electrostatic fields alone gave correct statistical result but clearly less than only steric fields. A grid spacing of 1 Å improved slightly the q^2 values for the same number of components. The statistical q^2 values were not in this case dependent on the orientation of the aligned molecules in the coordinate system with an average

Table 2. q^2 Values Associated with Different Conditions and Field Types[a]

	2 Å			1 Å		
	SE q^2 (ONC)[b]	S q^2 (ONC)	E q^2 (ONC)	SE q^2 (ONC)	S q^2 (ONC)	E q^2 (ONC)
none/smooth	0.798(9)	0.767(8)	0.612(3)	0.803(8)	0.789(8)	0.642(8)
box/smooth	0.798(9)	0.767(8)	0.612(3)	0.803(7)	0.789(8)	0.642(8)
none/abrupt	0.781(9)	0.766(8)	0.612(3)	0.797(8)	0.789(8)	0.642(8)
box/abrupt	0.81(8)	0.805(6)	0.598(3)	0.814(8)	0.812(6)	0.688(9)

[a] S: steric field and E: electrostatic field. [b] ONC: optimum number of components.

Table 3. Results of the CoMFA Analysis with 2 Å Spacing, Box and Abrupt Methods

	cross-validation		final equation	
number of components	q^2	s	r^2	s
1	0.503	0.300		
2	0.673	0.246		
3	0.751	0.216		
4	0.791	0.199		
5	0.799	0.197		
6	0.805	0.195	0.891	0.146
7	0.797	0.201		
8	0.798	0.202		
9	0.785	0.210		
10	0.778	0.215		

q^2 value of 0.76 and a standard deviation of 0.03. The best results are obtained with the "box"/"abrupt" method for the two possible grid spacing.

Considering the remarks above, the retained 3D-QSAR study corresponds to the correlation with steric fields, obtained with a "box"/"abrupt" method and a grid spacing of 2 Å. The statistical results are summarized in Tables 1 and 3.

The graphic representation of the final equation (r^2 = 0.891, 6 components) shows essentially three regions. One region (Figure 5) close to the nitrogen of the 3-anilino fragment, called region A in the following discussion, shows the importance of a secondary amine at this position. Any substitution on this amine led to decrease the affinities (see compounds **73**−**75**) up to one logarithmic unit (**6** vs **74**). Another region, called region B in the following discussion, is around the position 3, 4, and 5 of the 3-anilino fragment (Figures 2 and 6). Region B is occupied not only by polar groups such as OH or CO_2H but also by hydrophobic atoms such as chlorine. The steric factor, in region B, is explained by an increase in the biological affinities with bulky groups

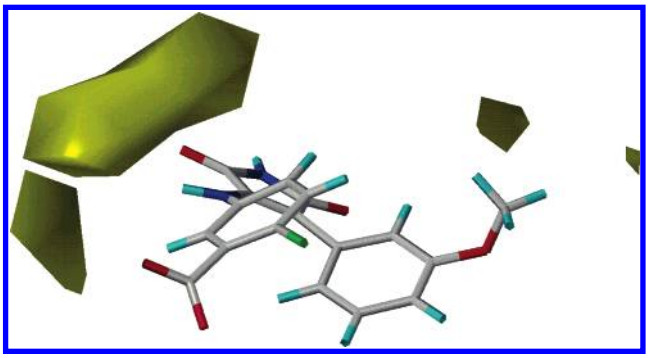

Figure 5. Standard deviation*PLS coefficients contour plots of CoMFA steric fields. Steric disfavored area (contribution level of 20%). Compound **51** inside the map.

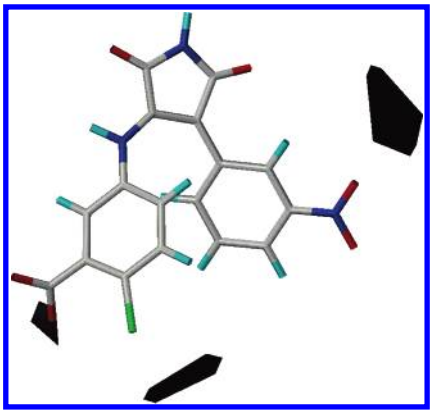

Figure 6. Standard deviation*PLS coefficients contour plots of CoMFA steric fields. Steric favored area (contribution level of 80%). Compound **52** inside the map.

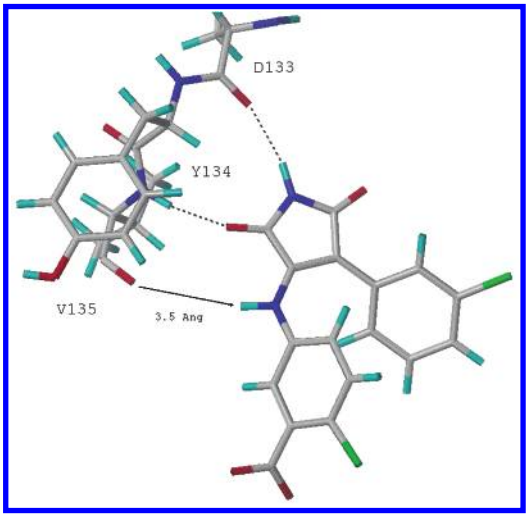

Figure 7. View (PDB ID: 1Q4L) of cocrystallographic data corresponding to region A of CoMFA study.

such as 3,5-dichloro-4-hydroxy (**42**) compared to 3-carboxy-4-chloro (**52**) or 3-chloro-4-hydroxy (**34**).

The last regions, called region C in the following discussion, are positioned around the 4-phenyl group. One region is characterized by the improvement of the affinity for the 3-nitro group compared to the 3-chlorine for instance (Figure 6). Steric factors ($E_s(Cl)$[32] = −0.97 vs $E_s(NO_2)$ = −2.52) can account for this result, but an electrostatic interaction of the nitro group with the active site or an electronic effect on the phenyl group ($\sigma_m(NO_2)$[32] = 0.71 vs $\sigma_m(Cl)$ = 0.37) could play an important role. In the last case, however, a 4-nitro group should get the same biological result (comparison of $\sigma_m(NO_2)$[32] and $\sigma_p(NO_2)$), and this was not observed (**42** vs **45**). The second region (Figure 5) is exemplified by a decrease in the affinity observed with 3-methoxy group (**51** vs **52** or **42** vs **47**).

In light of these analyses, it is interesting to compare the CoMFA results with the interactions observed in the cocrystallographic data between **50** and GSK-3β.

CoMFA Results and the Active Site of GSK-3β. The first region (corresponding to region A in the CoMFA study) displayed in Figure 7 shows two hydrogen bonds between the maleimide group and two residues in the active site (D133-Y134). These interactions are present for all the derivatives in the CoMFA study and must be important for the affinities. In addition, the aniline NH group of **50** was

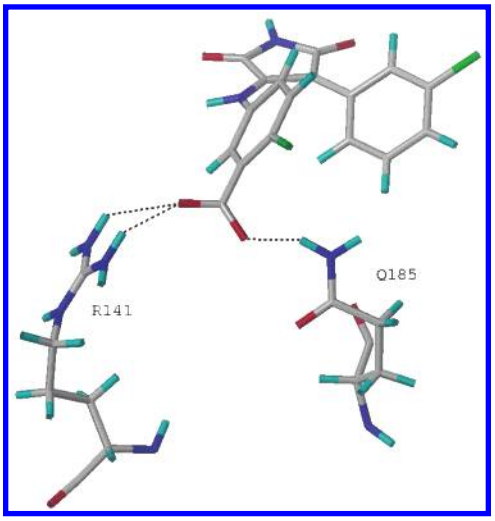

Figure 8. View (PDB ID: 1Q4L) of electrostatic interactions between **50** and R141, Q185.

found to be close to the V135 carbonyl group. The distance (3.5 Å) is being to large to represent a hydrogen bond. This distance is a priori compatible with a position of a methyl group in this area without forcing a different orientation of the molecule due to steric effects. However a drop of pIC_{50} is observed when a methyl group is present. This confirms the hydrophilic/hydrophobic character of this interaction.

Region B in CoMFA study was divided in two areas. The first one corresponds to the position associated with a carboxyl group for some derivatives. As illustrated in Figure 8, the carboxyl group of **50** interacts with two polar residues forming strong electrostatic interactions. It is worth noticing that a chlorine atom in the same position did not decrease the affinity. A particular conformation of the arginine residue (R141) was observed in this complex with a dihedral angle (CO-Cα-Cβ-Cγ) of 71.2° instead of a value around 180° in other cocrystallographic complexes. The same particular value for the dihedral angle (CO-Cα-Cβ-Cγ) was observed for Q185. These preferential conformations are explained by electrostatic interactions with the acidic function of the ligand. A histogram (see Figure 9), corresponding to an analysis of the Cambridge Structural Database,[33] shows the two main groups of values for this dihedral angle. With a chlorine atom at the same position, the residues R141 and/or Q185 should have a conformation close to those observed with other cocrystallographic data (PDB ID: 1Q41 and 1Q3W). A reinforcement of hydrophobic interactions with nonpolar residue like L188 (Figure 10) explains in this case the conservation of the biological affinity. The second area of region B, close to a chlorine atom (Figure 6), corresponds here to favorable interactions with the hydrophobic residues in the active site (I62, V70). In summary, region B incorporates an electrostatic interaction with R141/Q185 and a steric/hydrophobic factor with aliphatic residues.

In region C, when a nitro group (**52**) is substituted by a chloro group (**50**), while keeping the CoMFA alignment, two close contacts are observed with the side chain of K85 (Figure 11) and the backbone of S66 via the NH group. The nature of these interactions is electrostatic. The distance with the amino group of K85 is around 2.5 Å for an optimum theoretical distance of 2.1 Å.[34] This analysis shows that the steric factor associated with CoMFA study is in fact an electrostatic interaction. Finally, substitution by methoxy group in position 3 can lead to a steric hindrance with V70.

Comparison of Compound 1 and 3-Anilino-4-arylmaleimide Derivatives inside the Binding Site. The docking of **1** inside the binding site was the starting point for the comparison with the 3-anilino-4-arylmaleimide derivatives used. Using the crystallographic data (1Q4L) obtained with **50,** only a single orientation of **1** was obtained with hydrogen bonds between the 2-methoxyphenol fragment and the couple R141, V135 (Figure 12). However, the analysis of the RMS deviation between the residues inside the active site, by considering all cocrystallographic data, shows that the conformation of R141 is observed only in 1Q4L (as explained above, in relation with an acidic function on **50**).

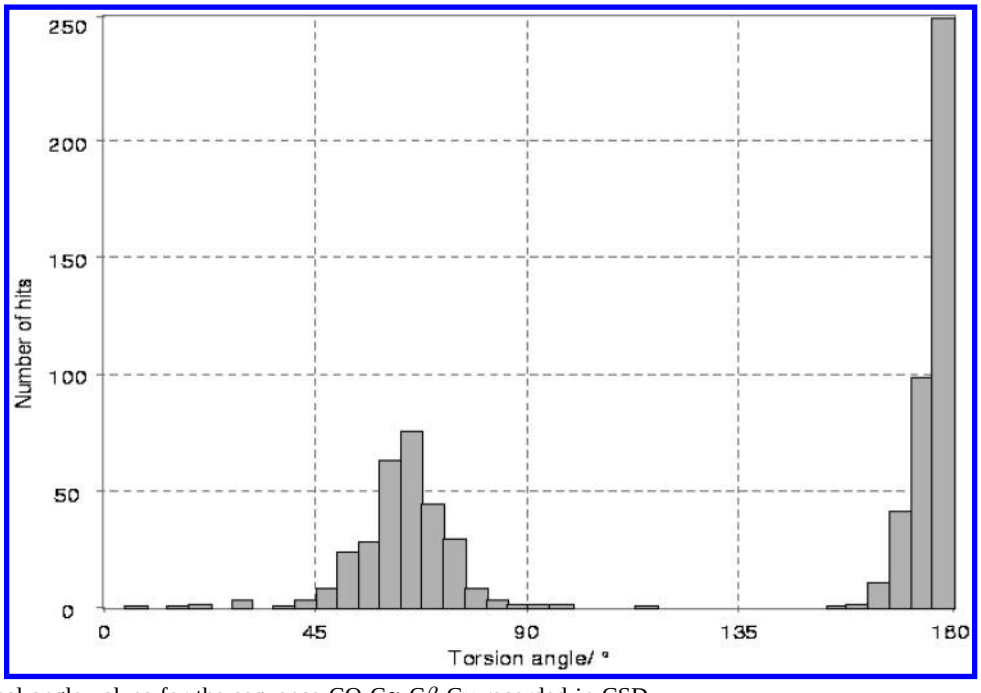

Figure 9. Torsional angle values for the sequence CO-Cα-Cβ-Cγ recorded in CSD.

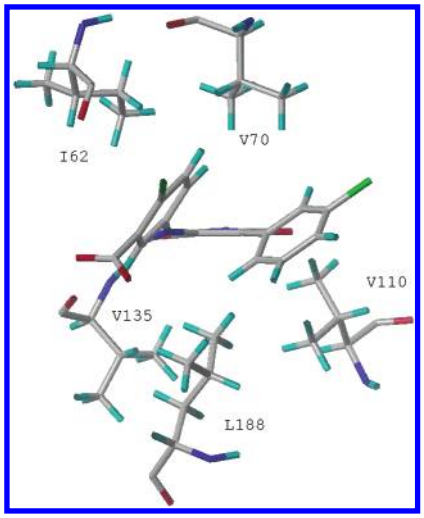

Figure 10. View (PDB ID: 1Q4L) of hydrophobic interactions between **50** and the active site, corresponding to region B of CoMFA study.

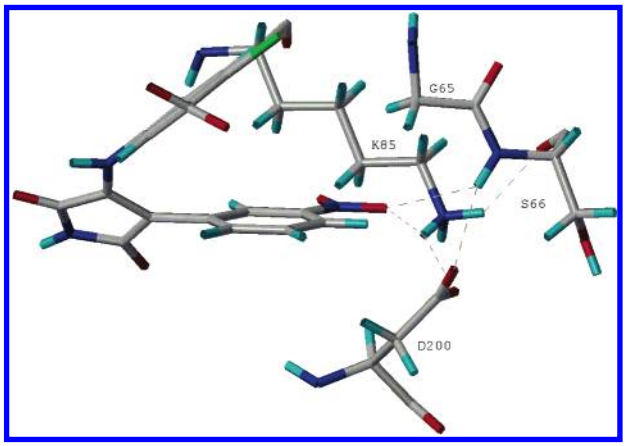

Figure 11. View (PDB ID: 1Q4L) corresponding to region C of CoMFA study with compound **52**.

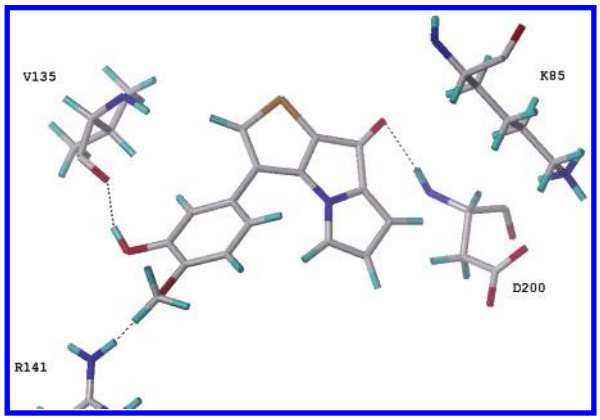

Figure 12. Orientation of **1** into the active site resulting from docking study starting from 1Q4L (PDB ID).

The overall RMS deviation for the backbone, corresponding to residues at 10 Å around the ligands, was ca. 0.3 Å.

GOLD performs automated docking with full acyclic ligand flexibility, partial cyclic ligand flexibility, and partial protein flexibility in the neighborhood of the protein active site.[27] However, the dihedral angles of residues R141 and Q185 could not be modified during the docking process by the program. In this case, two possibilities arise. Either the dihedral angles of residues R141 and Q185 are modified and the docking takes place, or another starting complex is used. In the last case, complexes with indirubin-3′-monoxime (PDB ID: 1Q41) or asterpaullone (PDB ID: 1Q3W) appear to be the most interesting. Indeed, the residues of the active site are relatively close (see Table 4), and the size and nature of the ligands are closer to **1** compared to staurosporine (PDB ID: 1Q3D) or Amp-PnP (PDB ID: PY1X). We chose to carry out the docking by starting from the cocrystallographic data with indirubin-3′-monoxime.

Table 4. RMSD (Å) between the Main Residues Inside the Active Site for Three Cocrystallographic Data (PDB ID)

	1Q41/1Q3W	1Q41/1Q4L	1Q3W/1Q4L
I62	0.19	0.13	0.29
G63	0.02	0.13	0.11
D64	0.64	0.58	0.25
G65	0.17	0.07	0.18
S66	0.16	0.69	0.79
V70	0.14	0.05	0.17
A83	0.01	0.05	0.04
I84	0.06	0.04	0.07
K85	0.17	0.13	0.19
M101	0.60	0.13	0.69
V110	0.09	0.97	1.04
R111	0.38	0.57	0.41
L112	0.11	0.09	0.07
L130	0.06	0.13	0.10
L132	0.16	0.04	0.04
D133	0.25	0.09	0.17
Y134	0.12	0.11	0.19
V135	0.03	0.05	0.03
R141	0.34	1.20	1.07
Q185	0.03	1.53	1.54
N186	0.07	0.11	0.07
L188	0.03	0.06	0.04
C199	0.03	0.09	0.10
D200	0.21	0.15	0.20
P201	0.04	0.04	0.05

The compound **1** adopted two possible orientations during docking when starting with 1Q41. In the first one (Figure 13), the 2-methoxyphenol fragment forms hydrogen bonds

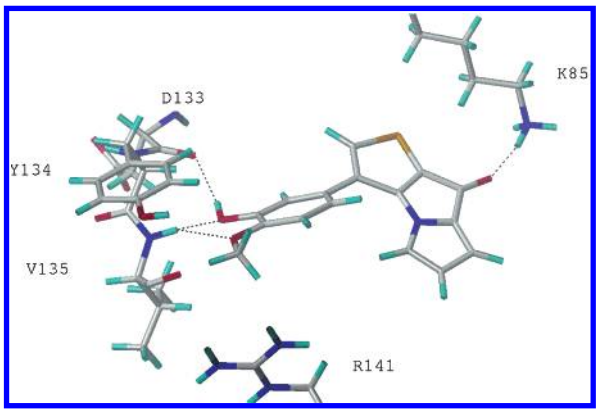

Figure 13. First orientation resulting from docking study starting from 1Q41 (PDB ID).

with the backbone of the sequence D133-Y134-V135. The oxygen of the carbonyl group of **1** forms electrostatic interactions with the amino group of K85 (the strength of this interaction is nearly the same as those with a nitro group[34]). We observed also a close contact between the aromatic sulfur and the alkyl chain of K85 through a hydrophobic interaction. The second orientation (Figure 14) corresponds to a rotation of nearly 180° compared to the first one with interactions between the 2-methoxyphenol

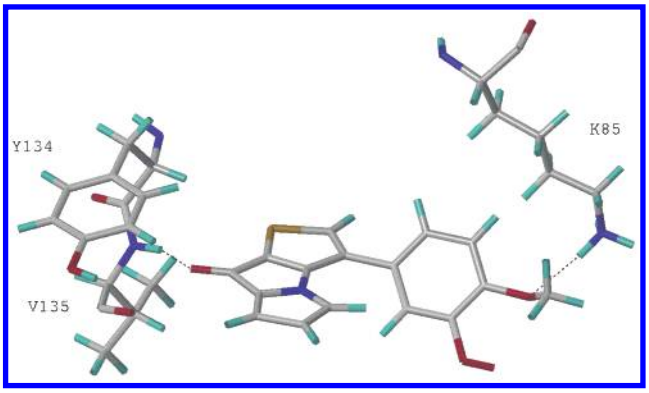

Figure 14. Second orientation resulting from docking study starting from 1Q41 (PDB ID).

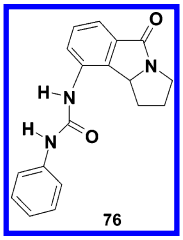

Figure 15. Compound **76** described as CDK-4 inhibitor.

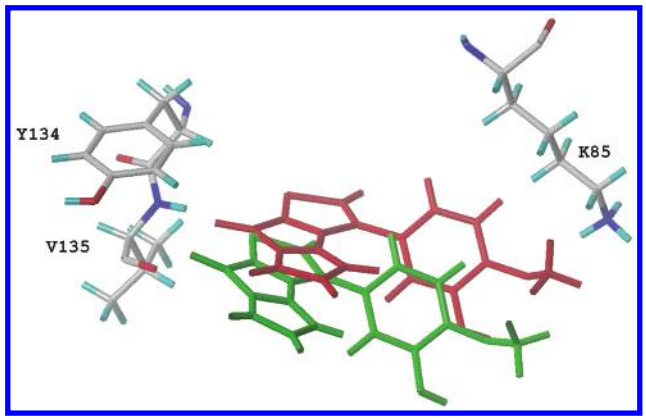

Figure 16. Variation of position of **1** during the minimization study (up: initial position; down: final position).

fragment and K85 of the active site, the carbonyl group forming hydrogen bonds with the sequence D133-Y134-V135.

Two arguments are in favor of the first orientation. The first one is based on one cocrystallographic data with a CDK-4 complex[35] between a compound named **76** (Figure 15), which has the same type of tricyclic feature than our derivative. The three-dimensional conformations of the active sites (GSK-3β vs CDK4 backbones) are conserved. Inside the active site, a Lys residue is conserved, and the sequence D133-Y134-V135 of GSK-3 is equivalent in CDK4 (E133-F134-L135) in terms of amino acid types. This compound shows an experimental orientation similar to the first one. The second is derived from the results of the energy minimization of the two complexes, corresponding to the two orientations, in solutions. After minimization, the RMSD results show that the position of **1** for the first orientation is rather conserved (RMSD = 0.23 Å), whereas it changes significantly for the second orientation as shown by the RMSD of 2.76 Å (Figure 16). This demonstrates that the second orientation obtained initially by docking does not seem to correspond to a local minimum in the presence of water. The total interaction energy is larger for the second orientation, and the compound **1** interacts in a greater extent in the first orientation with the active site (Table 5).

Table 5. Energy Interactions of Compound **1** (kcal/mol) after Minimization

	E_{TOTALE}	$E_{PROT/WATER/1}$	$E_{WATER/1}$	$E_{PROT/1}$
first orientation	−145870	−56.84	−3.21	−53.63
second orientation	−145828	−62.01	−13.2	−48.81

CONCLUSION

In this study, we first carried out a new 3D-QSAR study on selective inhibitors of GSK-3β yielding correct statistical results. We demonstrated than the results of the CoMFA analysis does not really correspond to the interactions recorded in the active site, but they characterize fundamental features (areas of the active site) of the interactions ligand−receptor. In undergoing docking studies, we were able to compare the position of our ligand with the 3-anilino-4-arylmaleimides derivatives. Additionally, we analyzed the results of the docking from several cocrystallographic data and revealed the interest of a minimization approach in solution to estimate the quality of the final orientation of the ligand. This led to a straight comparison with the reference compounds (Figure 17), explaining its affinity, and could serve to propose some pharmacomodulations.

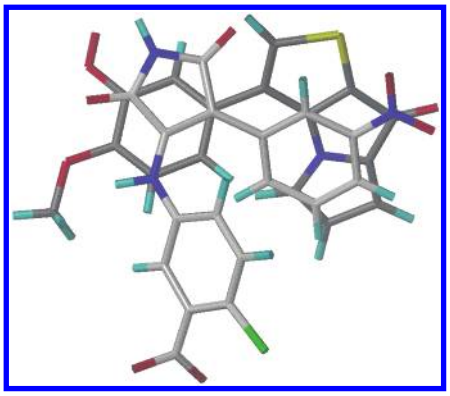

Figure 17. Superimposition of compounds **1** and **52**.

ACKNOWLEDGMENT

We thank the team of Professor Laurent Meijer (Cell Cycle Group, Station Biologique CNRS, BP 74, 29682 Roscoff cedex France) for the biological tests of our derivatives. We thank the CRIHAN (Centre de ressources informatiques de Haute Normandie) and the European Community (FEDER) for the molecular modeling software.

REFERENCES AND NOTES

(1) Cross, D. A.; Alessi, D. R.; Cohen, P.; Andelkovich, M.; Hemmings, B. A. Inhibition of glycogen synthase kinase-3 by insulin mediated by protein kinase B. *Nature* **1995**, *378*, 785−789.
(2) Hoeflich, K. P.; Luo, J.; Rubie, E. A.; Tsao, M. S.; Jin, O.; Woodgett, J. R. Requirement for glycogen synthase kinase-3β in cell survival and NF-B activation. *Nature* **2000**, *406*, 86−90.
(3) Ali, A.; Hoeflich, K. P.; Woodgett, J. R. Glycogen synthase kinase-3: properties, function and regulation. *Chem. Rev.* **2001**, *101*, 2527−2540.
(4) Doble, B. W.; Woodgett, J. R. GSK-3: tricks of the trade for a multi-tasking kinase. *J. Cell. Sci.* **2003**, *116*, 1175−1186.
(5) Loverstone, S.; Reynolds, C. H.; Latimer, D.; Davis, D. R.; Anderson, B. H.; Gallo, J.-M.; Hanger, D.; Mulot, S.; Marquardt, B.; Stabel, S.; Woodgett, J. R.; Miller, C. C. J. Alzheimer's disease-like phospho-

rylation of the microtubule-associated protein tau by glycogen synthase kinase-3 in transfected mammalian cells. *Curr. Biol.* **1994**, *4*, 1077−1086.
(6) Smith, G. D.; Buffet, M.; Fenwick, A. E.; Haigh, D.; Ife, R. J.; Saunders: M.; Slingsby, B. P.; Stacy, R.; Ward, R. W. 3-anilino-4-arylmaleimides: Potent and selective inhibitors of glycogen synthase kinase-3 (GSK-3). *Bioorg. Med. Chem. Lett.* **2001**, *11*, 635−639.
(7) Coghlan, M. P.; Culbert, A. A.; Cross, D. A. E.; Corcoran, S. L.; Yates, J. W.; Pearce, N. J.; Rausch, O. L.; Murphy, G. J.; Carter, P. S.; Cox, L. R.; Mills, D.; Brown, M. J.; Haigh, D.; Ward, R. W.; Smith, D. G.; Murray, K. J.; Reith, A. D.; Holder, J. C. Selective small molecule inhibitors glycogen synthase kinase-3 modulate glycogen metabolism and gene transcription. *Chem. Biol.* **2000**, *7*, 793−803.
(8) Kuo, G. H.; Prouty, C.; DeAngelis, A.; Shen, L.; O'Neill, D. J.; Shah, C.; Connoly, P. J.; Murray, W. V.; Conway, B. R.; Cheung, P.; Westover, L.; Xu, J. Z.; Look, R. A.; Demarest, K. T.; Emanuel, S.; Middleton, S. A.; Jolliffe, L.; Beavers, M. P.; Chen, X. Synthesis and discovery of macrolytic polyoxygenated bis-7-azaindolylmaleimides as novel series and highly selective glycogen synthase kinase-3β Inhibitors. *J. Med. Chem.* **2003**, *46*, 4021−4031.
(9) Zhang, H. C.; White, K. B.; Ye, H.; McComsey, D. F.; Derian, C. K.; Addo, M. F.; Andrade-Gordon, P.; Eckardt, A. J.; Conway, B. R.; Westover, L.; Xu, J. Z.; Look, R.; Demarest, K. T.; Emanuel, S.; Maryanoff, B. E. Macrocyclic bisindolylmaleimides as inhibitors of protein kinase C and glycogen synthase kinase-3. *Bioorg. Med. Chem. Lett.* **2003**, *13*, 3049−3053.
(10) Leclerc, S.; Garnier, M.; Hoessel, R.; Marko, D.; Bibb, J. A.; Snyder, G. L.; Greengard, P.; Biernat, J.; Wu, Y. Z.; Manderlkow, E. M.; Eisenbrand, G.; Meijer, L. Indirubins inhibit glycogen synthase kinase-3β and CDK5/P25, two protein kinases involved in abnormal tau phosphorylation in Alzheimer's disease. A property common to most cyclin-dependent kinase inhibitors. *J. Biol. Chem.* **2001**, *276*, 251−260.
(11) Loest, M.; Schultz, C.; Link, A.; Wu, Y. Z.; Biernat, J.; Mandelkow, E. M.; Bibb, J. A.; Snyder, G. L.; Greengard, D. W.; Zaharevitz, D. W.; Gussio, R.; Senderowicz, A. M.; Sausville, E. A.; Kunick, C.; Meijer, L. Paullones are potent inhibitors of glycogen synthase kinase-3β and cyclin-dependent kinase 5/p25. *Eur. J. Biochem.* **2000**, 267, 5983−5994.
(12) Kunick, C.; Lauenroth, K.; Leost, M.; Meijer, L.; Lemcke, T. 1-Azakenpaullone is a selective inhibitor of glycogen synthase kinase-3β. *Bioorg. Med. Chem. Lett.* **2004**, *14*, 413−416.
(13) Olesen, P. H., Sorensen, A. R.; Urso, B.; Kurtzhals, P.; Bowler, A. N.; Ehrbar, U.; Hansen, B. F. Synthesis and in vitro characterization of 1-(4-aminofurazan-3-yl)-5-dialkylaminomethyl-1*H*-[1,2, 3]triazole-4-carboxylic acid derivatives. A new class of selective GSK-3 inhibitors. *J. Med. Chem.* **2003**, *46*, 3333−3341.
(14) Mettey, Y.; Gompel, M.; Thomas, V.; Garnier, M.; Leost, M.; Ceballos-Picot, I.; Noble, M.; Endicott, J.; Vierfond, J. M.; Meijer, L. Aloisines, a new family of CDK/GSK-3 Inhibitors. SAR study, crystal structure in complex with CDK2, enzyme selectivity, and cellular effects. *J. Med. Chem.* **2003**, *46*, 222−236.
(15) Meijer, L.; Thunnissen, A. M. W. H.; White, A. W.; Garnier, M.; Nikolic, M.; Tsai, L.; H.; Walter, J.; Cleverley, K. E.; Salinas, P. C.; Wu, Y. Z.; Biernat, J.; Manderlkow, E. M.; Kim, S. H.; Pettit, G. R. Inhibition of cyclin-dependent kinases, GSK-3β and CK1 by hymenialdisine, a marine sponge constituent. *Chem. Biol.* **2000**, *7*, 51−63.
(16) ter Harr, E.; Coll, J. T.; Austen, D. A.; Hsiao, H. M.; Swenson, L.; Jain, J. Structure of GSK-3β reveals a primed phosphorylation mechanism. *Nat. Struct. Biol.* **2001**, *8*, 593−596.
(17) Bax, B.; Carter, P. S.; Lewis, C.; Guy, A. R.; Bridges, A.; Tanner, R.; Pettman, G.; Mannix, C.; Culbert, A. A.; Brown, M. J. B.; Smith, D. G.; Reith, A. D. The structure of phosphorylated GSK-3β complexed with a peptide, FRATtide, that inhibits β-catenin phosphorylation. *Structure* **2001**, *9*, 1143−1152.
(18) Dajani, R.; Fraser, E.; Roe, S. M.; Yeo, M.; Good, V. M.; Thompson, V.; Dale, T. C.; Pearl, L. Structural basis for recruitment of glycogen synthase kinase 3β to the axin-APC scafford complex. *EMBO J.* **2003**, *22*, 494−501.
(19) Bertrand, J. A.; Thieffine, S.; Vulpetti, A.; Cristani, C.; Valsasina, B.; Knapp, S.; Kalisz, H. M.; Flocco, M. Structural characterization of the Gsk-3β active site using selective and nonselective ATP-mimetic inhibitors. *J. Mol. Biol.* **2003**, *333*, 393−407.
(20) Rochais, C.; Lescot, E.; Lisowski, V.; Lepailleur, A.; Sopkova-De Oliveira Santos, J.; Bureau, R.; Dallemagne, P.; Meijer, L.; Rault, S. Design, synthesis, biological evaluation and SAR study of thieno-pyrrolizinones, a new family of CDK/GSK-3 inhibitors. *J. Enzymol. Inh. Med. Chem.* **2004**, *19*, 585−593.
(21) Lisowski, V.; Léonce. S.; Kraus-Berthier. L.; Sopkova-de Oliveira Santos, J.; Pierré, A.; Atassi, G.; Caignard, D. H.; Renard, P.; Rault, S. Design, synthesis, and evaluation of novel thienopyrrolizinones as antitubulin agents. *J. Med. Chem.* **2004**, *47*, 1448−64.
(22) Sybyl 6.9, Tripos Inc., St. Louis, MO, 2003, http://www.tripos.com.
(23) Clark, M.; Cramer, R. D., III; Van Opdenbosch, N. Validation of the general purpose tripos 5.2 force field. *J. Comput. Chem.* **1989**, *10*, 982−1012.
(24) Bush, B. L.; Nachbar, R. B., Jr. Sample-distance partial least squares: PLS optimized for many variables, with application to CoMFA. *J. Comput.-Aided Mol. Des.* **1993**, *7*, 587−619.
(25) Wold, S.; Albano, C.; Dunn, C. W.; Ellund, U.; Esbensen, K.; Geladi, P.; Hellberg, S.; Johansson, E.; Lindberg, W.; Sjostrom, M. *Multivariate Data Analysis in Chemistry. Chemometrics: Mathematics and Statistics in Chemistry*; Reidel: Dordrecht, Netherlands, 1984.
(26) Cho, S. J.; Tropsha, A. Cross-validated r^2-guided region selection for comparative molecular field analysis: a simple method to achieve consistent result. *J. Med. Chem.* **1995**, *38*, 1060−1066.
(27) Jones, G.; Willett, P.; Glen, R. C.; Leach, A. R.; Taylor, R. Development and validation of a genetic algorithm for flexible docking. *J. Mol. Biol.* **1997**, *267*, 727−748.
(28) Brooks, B. R.; Bruccoleri, R.; Olafson, B.; States, D.; Swaminathan, S.; Karplus, M. CHARMM: a program for macromolecular energy, minimization and dynamics calculations. *J. Phys. Chem.* **1983**, *4*, 187−217.
(29) MacKerell, A. D., Jr.; Bashford, D.; Bellott, M.; Dunbrack, R. L., Jr.; Evanseck, J. D.; Field, M. J.; Fischer, S.; Gao, J.; Guo, H.; Ha, S.; Joseph-McCarthy, D.; Kuchnir, L.; Kuczera, K.; Lau, F. T. K.; Mattos, C.; Michnick, S.; Ngo, T.; Nguyen, D. T.; Prodhom, B.; Reiher, W. E., III.; Roux, B.; Schlenkrich, M.; Smith, J. C.; Stote, R.; Straub, J.; Watanabe, M.; Wiorkiewicz-Kuczera, J.; Yin, D.; Karplus, M. All-atom empirical potential for molecular modeling and dynamics studies of proteins. *J. Phys. Chem. B* **1998**, *102*, 3586−3616.
(30) Jorgensen, W. L.; Chandrashekar, J.; Madura, J. D.; Impey, R.; Klein, M. L. Refined TIP3P model for water. *J. Chem. Phys.* **1983**, *79*, 926−935.
(31) Jaguar 5.5, schrödinger Inc., Portland, OR, 1991−2000, http://www.schrodinger.com/Products/jaguar.html.
(32) Hansch, C.; Leo, A. *Exploring QSAR. Fundamentals and Applications in Chemistry and Biology;* ACS Professional Reference Book, American Chemical Society: Washington, DC, 1995.
(33) Bruno, I. J.; Cole, J. C.; Kessler, M.; Luo, J.; Sam Motherwell, W. D.; Purkis, L. H.; Smith, B. R.; Taylor, R.; Cooper, R. I.; Harris, S. E.; Orpen, A. G. Retrieval of crystallographically derived molecular geometry information. *J. Chem. Inf. Comput. Sci.* **2004**, *44*, 2133−2144.
(34) Bruno, I. J.; Cole, J. C.; Lommerse, J. P. M.; Rowland, R. S.; Verdonk, M. L. Isostar: A library of information about nonbonded interactions. *J. Comput.-Aided Mol. Des.* **1997**, *11*, 525−537.
(35) Honma, T.; Hayashi, K.; Aoyama, T.; Hashimoto, N.; Machida, T.; Fukasawa, K.; Iwama, T.; Ikeura, C.; Ikuta, M.; Suzuki-Takahashi, I.; Iwasawa, Y.; Hayama, T.; Nishimura, S.; Morishima H. Structure-based generation of a new class of potent CDK-4 inhibitors: new *de novo* design strategy and library design. *J. Med. Chem.* **2001**, *44*, 4615−27.

CI050008Y